Electrolyte flows under magnetic fields: Manning-like counterion condensation in one dimension

Yoav Tsori*
Department of Chemical Engineering, Ben-Gurion University of the Negev, Beer-Sheva, Israel

Hannes Uecker†
Institute for Mathematics, Carl von Ossietzky Universität Oldenburg, Oldenburg, Germany
(Dated: February 22, 2026)

We present a theoretical framework for unidirectional magnetohydrodynamic flow of dilute electrolytes under perpendicular magnetic fields. Starting from the Navier–Stokes equation coupled with the Poisson–Nernst–Planck formulation, we show that the problem admits a sequential decoupling: the Stokes equation is solved first to obtain the velocity profile, which defines a hydrodynamic potential entering the Nernst–Planck description of ions. This Lorentz-force-induced potential competes with electrostatic attraction and significantly alters ionic distributions. We analyze this mechanism in two canonical geometries. In planar Couette shear, it produces a Manning–Oosawa-like condensation transition in one dimension, a phenomenon absent in classical electrostatics. We derive an eigenvalue equation predicting a sharp threshold between counterion enrichment and depletion at the charged wall. In cylindrical Taylor–Couette flow, the same effect shifts the classical Manning criterion by a magnetic parameter, enabling tunable control of condensation. These findings extend Manning–Oosawa phenomenology to driven, non-equilibrium systems and provide a basis for magnetic manipulation of screening in electrolytes, with implications for microfluidics, electrochemical systems, and nonlinear boundary-value theory.

I. INTRODUCTION

Magnetohydrodynamics (MHD) couples the Navier-Stokes equations of fluid motion with Maxwell's equations of electromagnetism, leading to a rich set of nonlinear phenomena. It plays a pivotal role in plasma confinement in fusion devices [1], solar and astrophysical processes [2, 3], and geodynamo action in Earth's core [4]. Its applied importance spans energy conversion (MHD generators) [5], metallurgical processing [6], electromagnetic pumps and emerging microfluidic technologies [7–9]. Despite its broad utility, MHD remains mathematically challenging due to the strong coupling between flow and electromagnetic fields, motivating both analytical and computational research [10].

MHD of electrolytes is traditionally formulated in terms of momentum transport with electromagnetic body forces and Ohmic conduction, typically assuming bulk electroneutrality and treating the ionic distribution as uniform [8, 9, 11, 12]. Standard macroscopic MHD strictly assumes bulk electroneutrality and neglects electrostatic forces. In large systems, ionic densities are essentially equal to each other and to their common bulk value, matching this assumption. However, near charged interfaces, on the scale of the Debye length, electroneutrality breaks down.

We present a formulation of one-dimensional MHD for dilute electrolytes in unidirectional flow that explicitly captures this boundary layer [13]: the Lorentz force acting on mobile ions induces a *hydrodynamic potential* that couples the Poisson-Nernst-Planck system to the Stokes flow in a way that allows a sequential decoupling of the hydrodynamics from the electrostatics. Crucially, while the ionic density differences are confined to the microscale, the Lorentz force drives a macroscopic variation in the electrostatic potential.

Consequently, once the unidirectional velocity profile is solved from the Stokes equation, it generates a hydrodynamic potential whose competition with electrostatic attraction determines the steady counterion distribution via a modified Poisson-Boltzmann (PB) equation. This framework provides a self-consistent route to quantify magnetic control of ionic distributions.

Here we apply the new formulation to simple, analytically tractable geometries. We focus on counterion-only systems and analyze (i) planar Couette shear and (ii) concentric, infinitely long coaxial cylinders (Taylor-Couette flow without instabilities). Despite the simplicity of these flows, we uncover a Manning–Oosawa (MO)–like condensation transition in both cases, driven not by electrostatics alone but by the bulk magnetic forcing.

Manning-Oosawa condensation describes the partial neutralization of a highly charged cylindrical macroion by its counterions [14, 15]. Mathematically, it is a peculiarity of the two-dimensional (2D) logarithmic Coulomb potential: in infinite systems, there exists a critical line-charge parameter above which a finite fraction of counterions *condense* near the macroion [16], while below it they *run away* to infinity [17–20]. In contrast, in one-dimensional (1D) planar geometry, counterions are always bound (no condensation threshold), whereas in three-dimensional (3D) spherical geometry counterion entropy wins over electrostatic attraction and they escape (no bound state) [21–23]. Thus, the appearance of

* tsori@bgu.ac.il
† hannes.uecker@uol.de

a condensation threshold is a hallmark of 2D electrostatics and does not occur in 1D within the classical, purely electrostatic PB description [24, 25].

Within our MHD-PB framework, the magnetic field and flow jointly generate a hydrodynamic potential that supplements the electrostatic potential in the Boltzmann weight. This additional, spatially varying term, competes with the electrostatic attraction and can qualitatively change binding. We show that even in planar, one-dimensional shear (a geometry that classically lacks a condensation threshold), there emerges a sharp criterion separating a regime with finite counterion density at the wall from a regime in which counterions escape to infinity, i.e., an MO-like transition *in 1D*. In cylindrical geometry, the same mechanism leads to a shift of the classical Manning threshold by a dimensionless magnetic parameter.

These sharp criteria apply in the limit of infinite flows, i.e., when for instance the distance d of the walls confining the flows goes to infinity. For finite systems, there is a continuous transition between counterions bound to the wall and counterions driven away from the wall, occurring at some finite strength $B = B_c \sim 1/d^2$. We shall analyze in detail the behaviour of the ions distribution $n^+(x)$ for B near B_c.

Section II presents the MHD formulation and the emergence of a hydrodynamic potential in unidirectional flows. Section III analyzes planar Couette shear flow and establishes the magnetic-field–induced MO-like transition in one dimension, including the eigenvalue condition and near-critical behavior. Section IV treats the coaxial-cylinder geometry, deriving the shifted Manning criterion. Section V concludes with implications and prospects.

II. MHD OF DILUTE ELECTROLYTES IN UNIDIRECTIONAL FLOW

We consider the flow of incompressible dilute electrolytes past one or two surfaces under the influence of a magnetic field. The Navier-Stokes equation is [26]

$$\rho\left[\frac{\partial \mathbf{v}}{\partial t} + (\mathbf{v}\cdot\nabla)\mathbf{v}\right] = -\nabla p + \eta\nabla^2\mathbf{v} + \rho_e\mathbf{E} + \mathbf{j}\times\mathbf{B} - k_BT\nabla n^+; \qquad (1)$$

$\mathbf{v}$ is the liquid's velocity, ρ its mass density, n^+ the counterion number density, p the pressure, η the liquid viscosity, $\mathbf{E}$ and $\mathbf{B}$ the electric and magnetic fields, respectively, and $\mathbf{j}$ is the electric current density.

The terms with $\mathbf{E}$ and $\mathbf{B}$ originate from the Lorentz force experienced by an ion of charge q, $\mathbf{f}_\mathrm{L} = q\,(\mathbf{E}+\mathbf{v}\times\mathbf{B})$, which transfers to the liquid. We assume a salt-free electrolyte where the only mobile charges are the positive counterions released from the moving wall; we denote the local charge density as $\rho_e = qn^+$. The term $k_BT\nabla n^+$ corresponds to the osmotic pressure of an ideal counterion gas, where k_B is the Boltzmann constant and T the absolute temperature.

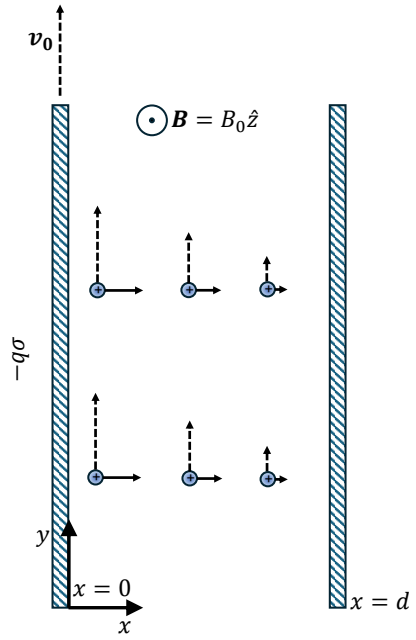

FIG. 1. System illustration. A liquid is confined between a surface at $x = 0$ ($-q\sigma$ charge density) moving at a speed v_0 in the y direction and a stationary surface at $x = d$. The liquid moves in unidirectional flow along y, dragging the positive counterions. An external magnetic field is applied in the z direction. Dashed arrows illustrate the local velocity; solid rightward arrows illustrate the Lorentz force $\mathbf{f}_L = q\,(\mathbf{E}+\mathbf{v}\times\mathbf{B})$ acting on counterions.

The total electrical current density is fundamentally the sum of the individual ionic fluxes, $\mathbf{j} = \sum q_i\mathbf{h}_i$, when there are several ionic species. In standard bulk MHD, this reduces to the classical Ohm's law, $\mathbf{j} = \sigma_e(\mathbf{E}+\mathbf{v}\times\mathbf{B})$. However, to capture the non-electroneutral boundary layer, we must retain the explicit Poisson-Nernst-Planck formulation. The ionic flux of counterions has three contributions: Lorentz force, diffusion, and advection with the liquid,

$$\mathbf{h} = n^+\mu q\,(\mathbf{E}+\mathbf{v}\times\mathbf{B}) - D\nabla n^+ + n^+\mathbf{v}, \qquad (2)$$

where μ is the ionic mobility in the liquid, $D = \mu k_BT$ is the diffusion constant, and $\mathbf{h}$ satisfies the Nernst-Planck equation

$$\partial_t n^+ + \nabla\cdot\mathbf{h} = 0. \qquad (3)$$

Our task is to solve (3) simultaneously with (1).

We focus on unidirectional flows such as the one illustrated in Fig. 1: A wall at $x = 0$ is charged with $-q\sigma$ charge per unit area, and moving vertically at a velocity v_0. σ is the surface charge number density. The wall at $x = d$ is stationary and uncharged. The fluid velocity is then $\mathbf{v} = v(x)\hat{y}$. In a constant perpendicular magnetic field, $\mathbf{B} = B_0\hat{z}$, and in the absence of electrochemistry

at the confining walls, $\mathbf{j}$ is parallel to $\hat{y}$, and both $\mathbf{E}$ and $\mathbf{j}\times\mathbf{B}$ are parallel to $\hat{x}$. In addition, because we assume a unidirectional velocity field of the form $\mathbf{v}=v(x)\hat{y}$, the nonlinear advection term $(\mathbf{v}\cdot\nabla)\mathbf{v}$ vanishes identically, regardless of the Reynolds number. The Navier-Stokes equations for the y component becomes the Stokes equation:

$$\rho\partial_t v(x) = -\partial_y p + \partial_x(\eta\partial_x v(x)). \tag{4}$$

Hence, the hydrodynamic problem in the y direction is the *same as if there are no magnetic and electric fields.* Consequently, once the flow profile $v(x)$ is found from (4), it can be substituted in (3) to find the ionic density $n^+(x)$.

We continue in steady state, where all time derivatives vanish. When the walls are impenetrable to ions ($h_x=0$ at the walls), the ion flux in the x-direction vanishes, namely

$$n^+\mu q\left(E+vB_0\right) - D\partial_x n^+ = 0, \tag{5}$$

where we used $\mathbf{E}=E\hat{x}$ and $(\mathbf{v}\times\mathbf{B})_x = vB_0$. In this problem, therefore, the ions' distribution is Boltzmann-like

$$n^+(x) = n_m \exp\left(\frac{-q\psi + U_{\rm hyd}(x)}{k_BT}\right), \tag{6}$$

where $n_m\equiv n^+(x=0)$ is the ion density at the moving wall (to be determined) and

$$U_{\rm hyd}(x) \equiv q\int_0^x v(x')B_0 dx' \tag{7}$$

is a hydrodynamic potential. For simple liquids and on the continuum level [27], the electrostatic potential ψ satisfies the Poisson equation $\nabla^2\psi = -qn^+/\varepsilon$, where ε is the dielectric constant of the liquid. Using the ion distribution in (6), we obtain a modified Poisson-Boltzmann equation

$$\nabla^2\psi = -\frac{qn_m}{\varepsilon}\exp\left(\frac{-q\psi+U_{\rm hyd}(x)}{k_BT}\right). \tag{8}$$

In the next section we turn to solve equations (4), (7), and (8) in planar Couette flow.

III. MANNING-OOSAWA-LIKE CONDENSATION IN COUETTE SHEAR FLOW

Due to the sequential decoupling between flow profile and ion density, in the Couette shear flow illustrated in Fig.1, we readily find that

$$\mathbf{v}(x) = v_0\left(1-\frac{x}{d}\right)\hat{y} \text{ and } U_{\rm hyd}(x) = qv_0B_0\left(x-\frac{1}{2}\frac{x^2}{d}\right).$$

The Poisson-Boltzmann equation and its boundary conditions are then

$$\psi'' = -\frac{qn_m}{\varepsilon}\exp\left(-\frac{q\psi}{k_BT}+\frac{qv_0B_0d}{k_BT}\left(\frac{x}{d}-\frac{1}{2}\frac{x^2}{d^2}\right)\right),$$
$$\psi'(0) = \frac{q\sigma}{\varepsilon}\ , \quad \psi'(d)=0.$$

It is instructive to use the dimensionless magnetic field $\tilde{B}$ and Bjerrum length defined as

$$\tilde{B} = qv_0B_0d/k_BT, \quad l_B = q^2/(\varepsilon k_BT),$$

and measure distances in units l_B, such that $\tilde{x}=x/l_B$ and $\tilde{d}=d/l_B$. Lastly, we define an auxilliary potential as $\phi = q\psi/k_BT - \tilde{B}\left(\tilde{x}/\tilde{d}-\tilde{x}^2/(2\tilde{d}^2)\right)$, leading to

$$\phi'' = -\lambda e^{-\phi} + \frac{\tilde{B}}{\tilde{d}^2}, \quad \lambda = l_B^3 n_m, \tag{9}$$
$$\phi'(0) = l_B^2\sigma - \frac{\tilde{B}}{\tilde{d}}\ , \quad \phi'(\tilde{d})=0, \quad \phi(0)=0,$$

where, without loss of generality, we set $\phi(0)=0$ because any constant shift in ϕ simply rescales λ, so fixing $\phi(0)=0$ ensures a unique nonlinear "eigenvalue" λ, which encodes the unknown n_m. The problem at hand is a nonlinear second-order ordinary differential equation with a constant "forcing" term, and one "additional" BC (three instead of two) compensated by the eigenvalue λ. The subtraction of the term proportional to $\tilde{B}$ in the definition of ϕ removes the explicit x-dependence in the exponential, simplifying the Poisson–Boltzmann equation to a form where the magnetic forcing appears as a constant term. Note that $\lambda = \frac{1}{2}l_B^2/\lambda_D^2$ if the Debye length λ_D is defined via $\lambda_D^2 = \varepsilon k_BT/(2n_mq^2)$, and that (9) yields the conservation integral

$$\int_0^{\tilde{d}} \lambda e^{-\phi} d\tilde{x} = l_B^2\sigma. \tag{10}$$

We start with a phase plane analysis of (9), based on the first order formulation

$$y_1' = y_2, \quad y_2' = -\lambda e^{-y_1} + \tilde{B}/\tilde{d}^2, \tag{11}$$

with "time" $\tilde{x}$ and conserved energy

$$E = \frac{1}{2}\phi'^2 + G(\phi), \quad G(\phi) = -\lambda \mathrm{e}^{-\phi} - \frac{\tilde{B}}{\tilde{d}^2}\phi. \tag{12}$$

From (10) we have $\lambda>0$, and the potential energy $G(\phi)$ has a unique maximum at

$$\phi_* = \ln(\lambda/\lambda^*) \quad \begin{cases} >0, & \lambda>\lambda^*, \\ <0, & \lambda<\lambda^*, \end{cases} \qquad \lambda^* = \tilde{B}/\tilde{d}^2. \tag{13}$$

Thus, for $\phi'(0) = l_B^2\sigma - \tilde{B}/\tilde{d} > 0$ we must have $\lambda>\lambda^*$, and for $\phi'(0)<0$ we obtain $0<\lambda<\lambda^*$, where the value of λ follows equivalently from $\phi'(\tilde{d})=0$ or from (10). For $\phi'(0)=0$ we have the unique solution $\phi\equiv 0$ with $\lambda=\lambda^*$. See Fig.2 ($\lambda>\lambda_*$) and Fig.3 ($\lambda<\lambda_*$) for illustration, where contrary to the role of λ as an eigenvalue depending on $\tilde{B},\tilde{d}$, and $\phi'(0)$, we a priori fix λ near λ_* and then vary $\phi'(0)$.

Since $G(\phi)$ has a unique maximum, $\phi(\tilde{x})$ must approach $\phi(\tilde{d})$ monotonically as $\tilde{x}\to\tilde{d}$. This implies that

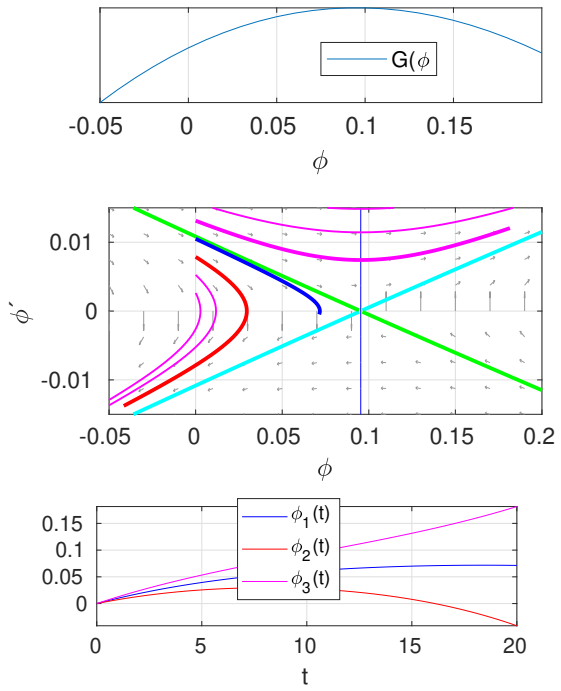

FIG. 2. Potential energy G, phase portrait, and selected solution curves for (9), $\tilde{B} = 5, \tilde{d} = 20$, $\lambda = 1.1\lambda_*$. The vertical blue line is at the fixed point $\phi_* = \ln(\lambda/\lambda_*)$, and the green/cyan lines illustrate the associated stable/unstable manifolds. We integrate (9) to $x = \tilde{d}$ with $\phi(0) = 0$ and varying $\phi'(0)$. The BC $\phi'(\tilde{d}) = 0$ means that we must land on the $\phi' = 0$ axis, which approximately holds for the blue curve. For illustration, we also show two "nearby" curves; the red curve reaches $\phi' = 0$ too early, and the (thick) magenta curve too late. Even for this relatively small $\tilde{d}$, the "correct" blue curve reaches $\phi' = 0$ close to the fixed point ϕ_*, hence with $\phi'' \approx 0$, see (14), (15).

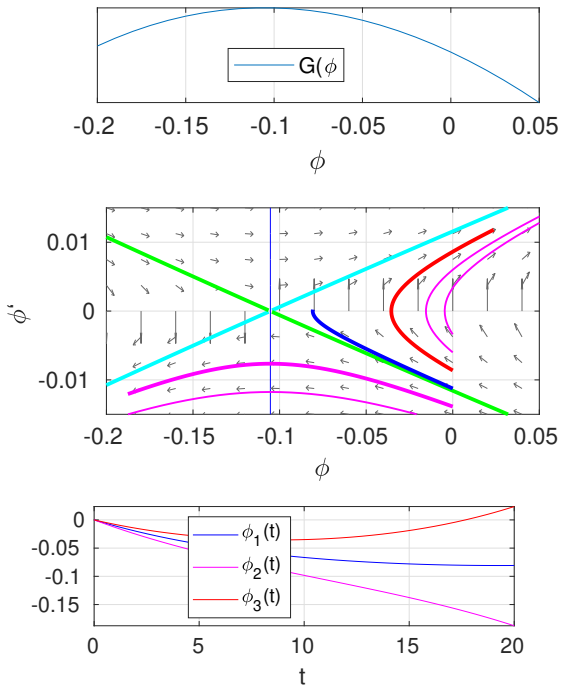

FIG. 3. Like Fig.2, but $\lambda = 0.9\lambda_*$. Hence fixed point at $\phi_* = \ln(\lambda/\lambda_*) < 0$, and initial conditions are chosen with $\phi'(0) < 0$.

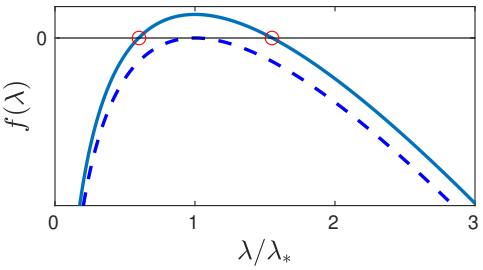

FIG. 4. Illustration of the approximate eigenvalue equation $f(\lambda) = 0$, with $f(\lambda)$ from (15). Dashed curve: $l_B^2\sigma = \tilde{B}/\tilde{d}$; Solid curve: $l_B^2\sigma \neq \tilde{B}/\tilde{d}$, with two roots $\lambda_1 < \lambda_* < \lambda_2$ (red circles).

for the first order formulation (11) and large $\tilde{d}$, the solution $\phi(\tilde{x})$ must be close to the stable manifold of the saddle point $(\phi, \phi') = (\phi_*, 0)$, which reaches $(\phi_*, 0)$ in infinite "time" $\tilde{x}$. In particular, $\phi(\tilde{d}) \approx \phi_* = \ln(\lambda/\lambda_*)$, and this allows to approximate λ via conservation of energy E. Namely,

$$\begin{aligned} 0 =& E(\tilde{x}{=}0) - E(\tilde{x}{=}\tilde{d}) \\ \approx& \frac{1}{2}\left(l_B^2\sigma - \frac{\tilde{B}}{\tilde{d}}\right)^2 - \lambda + \lambda_* + \lambda_* \ln(\lambda/\lambda_*), \end{aligned} \tag{14}$$

which yields an approximate (in the limit $\tilde{d} \to \infty$ with fixed $\tilde{B}/\tilde{d}$) equation for λ, namely

$$f(\lambda) := \lambda^* \left[1 + \ln\left(\frac{\lambda}{\lambda^*}\right) - \frac{\lambda}{\lambda^*}\right] + \frac{1}{2}\left(l_B^2\sigma - \frac{\tilde{B}}{\tilde{d}}\right)^2 = 0. \tag{15}$$

Figure 4 shows the shape of $f(\lambda)$; for $l_B^2\sigma = \tilde{B}/\tilde{d}$ we have a double root at $\lambda = \lambda_*$, while for $l_B^2\sigma \neq \tilde{B}/\tilde{d}$ we have two roots $\lambda_1 < \lambda_* < \lambda_2$. Again, from the phase portraits in Fig. 2 we see that for $\phi'(0) = l_B^2\sigma - \tilde{B}/\tilde{d} > 0$, the correct one is $\lambda_2 > \lambda_*$ because then $\phi_* = \ln(\lambda/\lambda_*) > 0$, while for $l_B^2\sigma - \tilde{B}/\tilde{d} < 0$ the correct one is $\lambda_1 < \lambda_*$. When $l_B^2\sigma = \tilde{B}/\tilde{d}$, the solution is $\phi \equiv 0$, and as $l_B^2\sigma - \tilde{B}/\tilde{d}$ decreases from positive to negative values, the potential at $\tilde{x} = \tilde{d}$ switches from $\phi(\tilde{d}) = \ln(\lambda_2/\lambda_*) > 0$ to $\phi(\tilde{d}) = \ln(\lambda_1/\lambda_*) < 0$.

The critical value of the normalized density

$$(l_B^2\sigma)_c = \frac{\tilde{B}}{\tilde{d}} = \frac{qv_0B_0l_B}{k_BT} \tag{16}$$

remains constant in the $\tilde{d} \to \infty$ limit. However, in this limit the critical value of λ tends to zero:

$$\lambda^* = \frac{\tilde{B}}{\tilde{d}^2} = \frac{qv_0B_0l_B^2}{k_BTd} \to 0. \tag{17}$$

For the counterion density $n^+(\tilde{x})=l_B^{-3}\lambda e^{-\phi(\tilde{x})}$ the above yields: In a finite system, there is always a finite value of λ, hence $n^+(0)=l_B^3\lambda$ at the left wall is finite. There is a critical value of the surface charge, $(l_B^2\sigma)_c = \tilde{B}/\tilde{d}$ where ϕ switches from increasing ($l_B^2\sigma > \tilde{B}/\tilde{d}$) to decreasing ($l_B^2\sigma > \tilde{B}/\tilde{d}$). Physically, it marks the point where the Lorentz-driven hydrodynamic potential exactly balances the electrostatic attraction. When $l_B^2\sigma < \tilde{B}/\tilde{d}$, the magnetic part of the Lorentz force is strong and counterions are depleted from the wall. In the limit $\tilde{d} \to \infty$, with fixed $\tilde{B}/\tilde{d}$, $\lambda_* = \tilde{B}/\tilde{d}^2 \to 0$, and for $l_B^2\sigma < (l_B^2\sigma)_c$ this implies that essentially $\lambda = 0$, i.e., the counterion density at the wall vanishes, and the solution corresponds to counterions escaping to infinity.

In the classical MO condensation, a counterion run-off threshhold occurs only in two-dimensions and not in one (counterions are always bounded) or three dimensions (counterions alway run off to infinity). Here, the transition occurs in one dimension due to the bulk (volume) force of magnetic origin. Moreover, irrespective whether $l_B^2\sigma - \tilde{B}/\tilde{d}$ is positive or negative, from $\phi(\tilde{d}) \approx \phi_* = \ln(\lambda/\lambda_*)$ the counterion density at $\tilde{x} = \tilde{d}$ is proportional to $\tilde{B}/\tilde{d}^2$ and tends to zero as $\tilde{d} \to \infty$.

To estimate the critical value of σ we use $q = e$, $v_0 = 0.1$m/s, $B_0 = 0.1$T, $l_B \approx 10$ nm and room temperature. One then finds a low critical charge density $(l_B^2\sigma)_c = \tilde{B}/\tilde{d} \approx 4 \times 10^{-9}$ indicating that usually a finite fraction of counterions will be bound to the surface.

Fig. 5 shows quantitative results for (9), and an assessment of the approximation (15). To numerically solve (9) for ϕ and λ we use the MATLAB solver `bvp5c` with λ as part of the solution, and to solve (15) we simply use `fzero`. In (a,b) we choose $(\tilde{d}, \tilde{B}) = (1000, 10)$, hence $\lambda_* = 10^{-5}$, and vary $l_B^2\sigma$. In (c) we plot λ as a function of $l_B^2\sigma$ for different $\tilde{d}$ values with fixed $\tilde{B}/\tilde{d} = 10^{-2}$; the full lines are from numerics, while the $\circ$ are from (15), with excellent agreement. For large $\tilde{d}$, λ is essentially 0 for $l_B^2\sigma < d/B$, and altogether all results fully agree with those explained (semi-)analytically above.

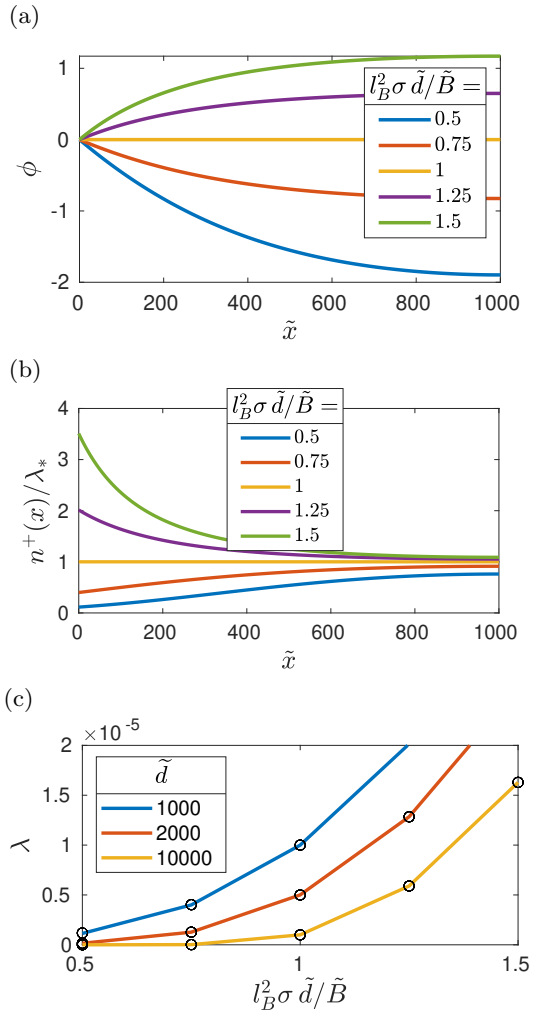

FIG. 5. (a,b) Profiles $\phi(\tilde{x})$ and $n_+(x)/\lambda_*$ for various values of $l_B^2\sigma$ and fixed $\tilde{d} = 10^3$ and $\tilde{B} = 10$. $\tilde{x} = x/l_B$ is the length in units of the Bjerrum length. (c) λ as a function of $l_B^2\sigma$ for different $\tilde{d}$ with fixed $\tilde{B}/\tilde{d} = 10^{-2}$; full numerics for (9) (lines) compared to numerical solution of (15) ($\circ$).

IV. ELECTROLYTES IN TAYLOR-COUETTE FLOW

We have found counterion run-off in one Cartesian dimension. Let us examine a two-dimensional system of two rotating cylinders and see how the classical transition is affected here. Figure 6 shows an electrolyte confined between two infinitely long coaxial cylinders with radii a and $b > a$. The inner one rotates at an angular frequency ω and is charged with $-q\sigma$ Coulomb per unit area (σ is a surface number density). Its counterions are released to the liquid. The outer cylinder is stationary and neutral. The magnetic field is oriented along the cylinders' axis, $\mathbf{B} = B_0\hat{z}$. Since ions move in the azimuthal direction, the electric field acts in the radial direction, $\mathbf{E} = E\hat{r}$.

Let us look at the magnitude of centrifugal force compared to the Lorentz force in the radial direction. The strongest acceleration v^2/r is at the inner cylinder, where $r = a$ and $v = \omega a$. Hence, the centrifugal force acting on an ion is $f_{\rm cent} = m_i\omega^2 a$, where m_i is the ionic mass. Assuming a Sodium ion (23 atomic mass units), $a = 1$ cm and $\omega = 100$ rad/s, we find $f_{\rm cent} \approx 4 \times 10^{-24}$N. The magnetic force for a unit charge moving at the same velocity (1 m/s) in a large magnetic field of 0.1 Tesla is $f_L = 1.6 \times 10^{-20}$N. With this estimate we safely neglect the effect of centrifugal acceleration.

It is useful to look at the steady Navier-Stokes equations in polar coordinates (r, θ) [28], i.e. for the (r, θ) components:

$$r: \quad -\rho\frac{v_\theta^2}{r} = -\partial_r p + \rho E + jB_0 - k_B T\partial_r(n^+ + n^-),$$

$$\theta: \quad 0 = \frac{1}{r^2}\partial_r\left(\eta r^3\partial_r\left(\frac{v_\theta}{r}\right)\right).$$

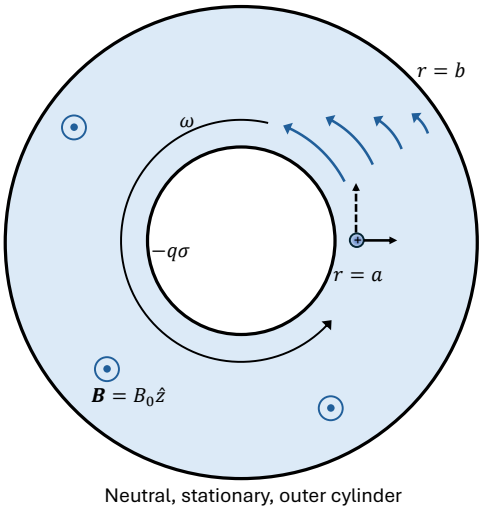

FIG. 6. Illustration of electrolyte (light blue) with positive counterions confined between two coaxial cylinders with inner and outer radii a and b, respectively. The inner cylinder has $-q\sigma$ surface charge density and rotates at a frequency ω while the outer one is stationary and electrically neutral. The magnetic field along the cylinders' axis (z direction) leads to a Lorentz force in the radial direction.

The total ionic flux $\mathbf{h}$ has two terms along $\hat{r}$ and advection along $\hat{\theta}$:

$$\mathbf{h} = \left[n^+\mu q\left(\mathbf{E}+\mathbf{v}\times\mathbf{B}\right) - D\nabla n^+\right]\hat{r} + n^+ qv\hat{\theta}.$$

As in the Cartesian case, the ionic flux vanishes in the r direction, and the r equation simplifies to $-\rho v_\theta^2/r = -\partial_r p$, yielding the pressure once v_θ is known from the θ direction. The flow profile solving the θ-equation is

$$\mathbf{v}(r) = \frac{\omega a}{1-\left(\frac{a}{b}\right)^2}\frac{a}{b}\left(-\frac{r}{b}+\frac{b}{r}\right)\hat{\theta}. \tag{18}$$

The continuity equation for the ionic flux $\nabla\cdot\mathbf{h}=0$ means that

$$\frac{1}{r}\frac{\partial(rh_r)}{\partial r}+\frac{1}{r}\frac{\partial h_\theta}{\partial\theta}+\frac{\partial h_z}{\partial z}=0,$$

and the cylindrical symmetry leads to

$$r\left[n^+\mu q\left(\mathbf{E}+\mathbf{v}\times\mathbf{B}\right) - D\nabla n^+\right]=0,$$

where we used the vanishing flux at the hard walls at $r=a$ and $r=b$. Integration of this equation gives the cation density as a Boltzmann-like distribution

$$n^+(r) = n_m\exp\left(\frac{-q\psi+U_{\rm hyd}(r)}{k_BT}\right),$$

where n_m is a yet-unknown constant and the hydrodynamic potential is $U_{\rm hyd}(r)\equiv q\int_a^r v(r')B_0dr'$ with $v(r)$ given by (18).

We now make a series of transformations: First, length is measured in units of a, $\tilde{r}=r/a$, and following Burak and Orland [18] we introduce the logarithmic coordinate

$$u=\ln(\tilde{r}) \text{ with } 0\le u\le d:=\ln(b/a) \tag{19}$$

to map the cylindrical domain to a rectangular one. We then define

$$\phi = \frac{q\psi}{k_BT}-\frac{\tilde{B}}{g}\left(-\frac{a}{2b}\tilde{r}^2+\frac{b}{a}\ln(\tilde{r}a/b)\right),$$

where

$$v_0=\omega a,\quad g=\frac{b}{a}-\frac{a}{b},\quad \tilde{B}=\frac{qv_0B_0a}{k_BT}.$$

Finally, we define φ as $\varphi=\phi-2u$, removing the explicit geometric and magnetic contributions. These steps yield the Poisson-Boltzmann equation

$$\varphi'' = -\lambda e^{-\varphi}+2\frac{\tilde{B}a}{gb}e^{2u}, \tag{20}$$
$$\varphi'(0)=l_B\sigma a-2-\tilde{B},\quad \varphi_u(d)=-2,\quad \varphi(0)=0.$$

As before, the last BC is a choice of the gauge, leading to a unique eigenvalue

$$\lambda = l_Bn_m'a^2 \tag{21}$$

for solving (20), where

$$n_m' = n_m\exp\left(\frac{\tilde{B}}{g}\left(\frac{a}{2b}+\frac{b}{a}\ln(\frac{b}{a})\right)\right).$$

The term $2\tilde{B}a/(gb)e^{2u}$ represents the inhomogeneous magnetic forcing arising from the hydrodynamic potential in cylindrical geometry. The different definition of λ (compared to Sec.III) arises from the geometry: cylindrical vs planar. Similarly, $\tilde{B}$ is divided by an additional geometric factor g in cylindrical coordinates, and the boundary conditions in (20) now yield the charge conservation

$$\int_0^d\lambda e^{-\varphi}du = l_B\sigma a. \tag{22}$$

Before we continue, let us make a short recap of the regular Manning-Oosawa (MO) condensation, recovered formally when $\tilde{B}=0$, occurring in the limit $\frac{b}{a}\to\infty$. Here, there are two scenarios: when $l_B\sigma a<2$, the eigenvalue λ essentially vanishes, and the (approximate, with violation of the right BC) solution then is $\varphi_0=(l_B\sigma a-2)u$, i.e, $q\psi_0/k_BT=l_B\sigma a\ln(r/a)$; – the counterions "run" to infinity. Since n_m, the concentration of counterions at the inner cylinder, is proportional to λ, their concentration vanishes. Above the Manning criterion, $l_B\sigma a>2$, $\varphi_0(u)=2\ln\left(1+\frac{1}{2}(l_B\sigma a-2)u\right)$ (and $\lambda=l_B\sigma a-2$). That is, $q\psi_0/k_BT=2\ln(r/a)+2\ln\left[1+\frac{1}{2}(l_B\sigma a-2)\ln(r/a)\right]$.

We now go back to the case with magnetic field. There is a transition analogous to the MO condensation: In the limit $\frac{b}{a}\to\infty$, $\lambda\approx0$ when $l_B\sigma a<2+\tilde{B}$. Counterions escape radially outward and run off to infinity like in the MO condensation. The MO criterion is shifted; the surface charge density is renormalized such

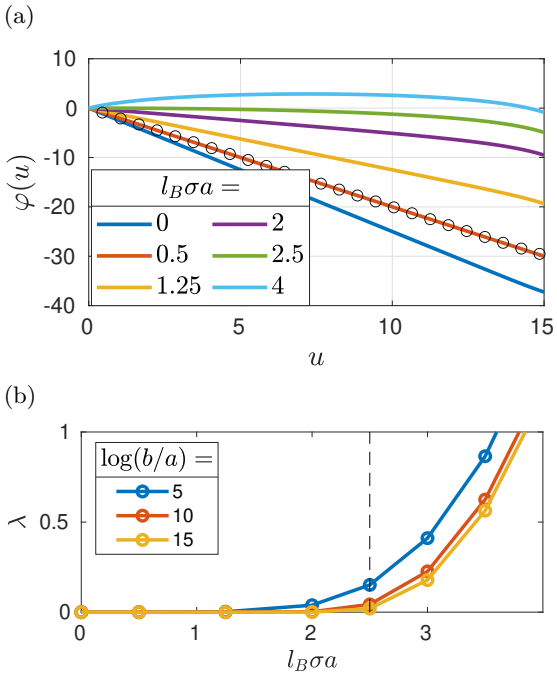

FIG. 7. (a) Solutions $\varphi(u)$ for selected values of $l_B\sigma a$, $\log(b/a) = 15$ and $\tilde{B} = 0.5$. Blue curve for $\lambda = 0$ is the approximation (23) with $l_B\sigma a = 0$, and circles are (23) for the smallest non-zero value, $l_B\sigma a = 0.5$. (b) λ from (20) vs $l_B\sigma a$ for different $\log(b/a)$, The vertical dashed line marks the shifted Manning threshold $l_B\sigma a{=}2 + \tilde{B}$.

that $l_B\sigma a^* = l_B\sigma a - \tilde{B}$. The additional $\tilde{B}$ term reflects the magnetic contribution to the effective surface charge. There is also a quantitative difference due to the inhomogeneous driving, but this is less essential to the condensation transition.

For finite b/a and $\lambda = 0$, an approximate analytical solution to (20) satisfying both $\varphi_u(0) = l_B\sigma a - 2 - \tilde{B}$ and $\varphi(0) = 0$ is

$$\varphi = \frac{1}{2}\frac{\tilde{B}a}{gb}e^{2u} + c_2 u + c_1, \tag{23}$$

with $c_2 = l_B\sigma a - 2 - \tilde{B}\left(1 + \frac{a}{gb}\right)$, and $c_1 = -\frac{1}{2}\frac{\tilde{B}a}{gb}$. The counterion concentration at the inner cylinder vanishes, and ions migrate outward indefinitely, similar to the MO runaway in cylindrical geometry. The mismatch of the right boundary condition in this case is the same as in the MO case.

Figure 7(a) shows selected profiles $\varphi(u)$, and comparison with (23) for the smallest non-zero surface charge value, $l_B\sigma a = 0.5$, giving excellent match with the numerical solution. Figure (b) shows the eigenvalue λ calculated numerically from (20) as a function of $l_B\sigma a$. When $l_B\sigma a > 2 + \tilde{B}$, λ is positive and $\varphi(u)$ is a concave function. When $l_B\sigma a$ decreases below $2 + \tilde{B}$, λ essentially vanishes for large b/a.

V. CONCLUSIONS

We presented a theoretical framework for MHD effects in electrolyte flows in a Stokes-Poisson-Nernst-Planck formulation, focusing on how magnetic forcing interacts with electrostatic screening to control ionic distributions. By introducing a hydrodynamic potential that competes with electrostatics, we extend classical MHD models beyond uniform conductivity and local electroneutrality assumptions. The analysis for unidirectional flows reveals novel mechanisms for magnetic control of screening [29] and identifies condensation-like transitions in driven systems.

Our results show that, even within the Stokes-Poisson-Nernst-Planck framework, magnetic forcing can reconfigure ionic distributions through a hydrodynamic potential. This goes beyond standard MHD models, providing a theoretical basis for magnetic control of screening in canonical flows [11, 30]. We identify a non-electrostatic route to MO-like transitions, including a condensation threshold in 1D (planar shear) and a shift of the classical Manning criterion for cylindrical geometries. This extends MO phenomenology to driven, non-equilibrium settings, while retaining analytical tractability within a modified PB theory [14, 15, 18, 20, 31].

For typical aqueous electrolytes at room temperature, the critical surface charge density required to observe the exact threshold is very low. However, the primary value of this work is establishing the fundamental existence of a non-geometric route to condensation. Furthermore, the transition is governed by the dimensionless parameter $\tilde{B} = qv_0B_0d/k_BT$. This parameter can be enhanced by several orders of magnitude to reach experimentally accessible regimes in specific soft-matter environments. For instance, in highly viscous systems like ionic liquids or polymer melts, larger velocity gradients can be maintained without triggering turbulence. Similarly, the use of multivalent ions, lower temperatures, or microfluidic devices with extremely strong local magnetic fields can push the system toward the transition threshold.

ACKNOWLEDGMENTS

We are grateful for financial support by the Israel Science Foundation Grant No. 332/24.

[1] J. Goedbloed and S. Poedts, *Principles of Magnetohydrodynamics: With Applications to Laboratory and Astrophysical Plasmas* (Cambridge University Press, Cambridge, UK, 2004).

[2] A. Srivastava, M. Goossens, and I. Arregui, *Magnetohydrodynamic Processes in Solar Plasmas* (Springer, Cham, 2024).

[3] E. Priest, *Magnetohydrodynamics of the Sun* (Cambridge University Press, 2014).

[4] P. Roberts and E. King, The geodynamo and the origin of earth's magnetic field, Rep. Prog. Phys. **76**, 096801 (2013).

[5] R. J. Rosa, *Magnetohydrodynamic Energy Conversion* (McGraw-Hill, New York, 1968).

[6] E. Matinde, Metallurgical slags: A drive to circularity and search for new research agenda, J. South Afr. Inst. Min. Metall. **124**, 491 (2024).

[7] H. H. Bau, Applications of magneto electrochemistry and magnetohydrodynamics in microfluidics, Magnetochemistry **8**, 140 (2022).

[8] N.-T. Nguyen, Micro-magnetofluidics: interactions between magnetism and fluid flow on the microscale, Microfluidics and Nanofluidics **12**, 1 (2012).

[9] N.-T. Nguyen, Special issue on magnetic-based microfluidics, Microfluidics and Nanofluidics **13**, 527 (2012).

[10] P. Davidson, *An Introduction to Magnetohydrodynamics*, 2nd ed. (Cambridge University Press, Cambridge, UK, 2016).

[11] U. Müller and L. Bühler, *Magnetofluiddynamics in Channels and Containers* (Springer, Berlin, 2001).

[12] T. Z. Fahidy, Magnetoelectrolysis, J. Appl. Electrochem. **13**, 553 (1983).

[13] M. Z. Bazant, Exact solutions and physical analogies for unidirectional flows, Phys. Rev. Fluids **1**, 024001 (2016).

[14] G. S. Manning, Limiting laws and counterion condensation in polyelectrolyte solutions I. Colligative properties, J. Chem. Phys. **51**, 924 (1969).

[15] F. Oosawa, *Polyelectrolytes* (Marcel Dekker, New York, 1971).

[16] J. G. Hedley, K. Coshic, A. Aksimentiev, and A. A. Kornyshev, Electric field of DNA in solution: Who is in charge?, Phys. Rev. X **14**, 031042 (2024).

[17] R. R. Netz and J.-F. Joanny, Complexation behavior of polyampholytes and charged objects, Macromolecules **31**, 5123 (1998).

[18] Y. Burak and H. Orland, Manning condensation in two dimensions, Phys. Rev. E **73**, 010501 (2006).

[19] R. R. Netz and H. Orland, Beyond poisson-boltzmann: Fluctuation effects and correlation functions, Eur. Phys. J. E **1**, 203 (2000).

[20] E. Trizac and G. Téllez, Onsager-Manning-Oosawa condensation phenomenon and the effect of salt, Phys. Rev. Lett. **96**, 038302 (2006).

[21] E. Trizac, L. Bocquet, and M. Aubouy, Simple approach for charge renormalization in highly charged macroions, Phys. Rev. Lett. **89**, 248301 (2002).

[22] L. Šamaj and E. Trizac, Counterions at highly charged interfaces: From one plate to like-charge attraction, Phys. Rev. Lett **106**, 078301 (2011).

[23] G. Ariel and D. Andelman, Polyelectrolyte persistence length: Attractive effect of counterion correlations and fluctuations, Europhys. Lett. **61**, 67 (2003).

[24] D. Andelman, Introduction to electrostatics in soft and biological matter, Soft condensed matter physics in molecular and cell biology **6**, 97 (2006).

[25] P. S. Kuhn, Y. Levin, and M. C. Barbosa, Rodlike polyelectrolytes in the presence of monovalent salt, Macromolecules **31**, 8347 (1998).

[26] R. F. Probstein, *Physicochemical Hydrodynamics: An Introduction* (John Wiley & Sons, Hoboken, NJ, 2003).

[27] M. V. Fedorov and A. A. Kornyshev, Ionic liquid near a charged wall: Structure and capacitance of electrical double layer, J. Phys. Chem. B **112**, 11868 (2008).

[28] R. B. Bird, W. E. Stewart, and E. N. Lightfoot, *Transport Phenomena*, 2nd ed. (John Wiley & Sons, New York, 2002).

[29] A. A. Kornyshev, Double-layer in ionic liquids: paradigm change?, J. Phys. Chem. B **111**, 5545 (2007).

[30] S. Qian and H. H. Bau, Magneto-hydrodynamics based microfluidics, Mech. Res. Commun. **36**, 10 (2009).

[31] Y. Levin, Kosterlitz–Thouless and Manning condensation, Physica A: Statistical Mechanics and its Applications **257**, 408 (1998).